

High resolution vibration-rotation emission spectroscopy of BaH

By KALEY A. WALKER, HARTMUT G. HEDDERICH, and
PETER F. BERNATH†

Centre for Molecular Beams and Laser Chemistry, Department of Chemistry,
University of Waterloo, Waterloo, Ontario, Canada N2L 3G1

(Received 13 July 1992; accepted 13 July 1992)

The high resolution infrared emission spectrum of barium monohydride was recorded. The fundamental and two hot band transitions were measured for the main isotopic species ^{138}BaH , and the fundamental band was measured for the minor isotopic species ^{137}BaH , ^{136}BaH , and ^{135}BaH . Improved Dunham constants were determined for all four isotopomers. The sensitivity of the infrared emission technique was demonstrated by the improved accuracy of the Dunham constants.

1. Introduction

The rovibrational transitions of barium monohydride (BaH) have not been studied extensively, unlike the electronic transitions involving the $\text{X}^2\Sigma^+$ ground state. BaH is a free radical which can be produced by the reaction of barium metal and hydrogen at high temperatures.

BaH was first investigated by Fredrickson and Watson in 1932 [1] in the red region of the spectrum where the $\text{E}^2\Pi \rightarrow \text{X}^2\Sigma$ electronic transition was studied. Since that time there have been many additional experimental studies [e.g. 2,3] and one *ab initio* calculation [4] of the electronic spectra. In 1988, Magg, Birk and Jones recorded the vibration-rotation spectrum of BaH [5]. In their study, the BaH radical was generated using a tube furnace, and an absorption spectrum was recorded using a tunable diode laser system. This work was the first to measure the transitions of isotopic species other than the most abundant ^{138}BaH (72%). The main disadvantage of the diode laser technique is the limited operating range, resulting in small data sets.

We have found that Fourier transform emission spectroscopy is an excellent technique for measuring the spectra of high temperature molecules. This emission technique has a wider spectral coverage and is more precise and accurate than diode laser absorption spectroscopy, because of the use of a Fourier transform spectrometer. Unfortunately, Fourier transform emission spectroscopy is less sensitive than diode laser absorption spectroscopy but it is, nevertheless, more sensitive than traditional infrared absorption spectroscopy.

2. Experimental

Barium hydride was produced in the gas phase using a tube furnace system. A 1 m stainless steel tube was heated by eight clamshell heaters. The barium metal was placed on a stainless steel wire gauze pad in the centre of the heating region to ensure that the metal remained in this region when in the liquid state. The temperature of the

† Also: Department of Chemistry, University of Arizona, Tucson, Arizona 85721, U.S.A.

tube was measured by a chromel–alumel thermocouple inserted between the tube and the heaters.

To prepare for the experiment, the barium metal was heated under vacuum to 650 °C to remove gases from the furnace. To record the spectrum, the barium metal was then heated under a vacuum to 700 °C. The pumping port was closed and heating was continued to 900 °C. Hydrogen at 20 Torr was added through the gas inlet to the tube furnace and the heating was continued to 1000 °C. Both the pumping port and the gas inlet were closed while the spectrum was recorded. It was found that the hydrogen gas must be added at a temperature much higher than the melting point of barium (725 °C) because a compound, probably barium dihydride, forms rapidly when the hydrogen is added at lower temperatures. At higher temperatures, the barium dihydride decomposes and the pressure of hydrogen rises rapidly in the tube furnace. Rather than trying to control the pressure in the furnace by pumping away the excess hydrogen, it was easier to add the hydrogen above 900 °C and avoid the formation of the dihydride.

At 1030 °C, the spectrum of the hot barium monohydride was recorded in emission using a Bruker IFS 120 HR Fourier transform spectrometer. A liquid nitrogen cooled HgCdTe detector and a KBr beamsplitter were used. The unapodized resolution was 0.005 cm⁻¹ over a spectral range of 900–1700 cm⁻¹. The upper wavelength limit was set by a red pass optical filter, and the lower wavelength was set by the CaF₂ windows and the detector response. One hundred scans were taken over 4 h and co-added.

A calibration spectrum was recorded under the same experimental conditions as the BaH spectrum. When the BaH spectrum was completed, D₂O was added to the cell and a calibration spectrum was measured, in absorption, using a globar source. The D₂O reacted quickly with the contents of the tube furnace, so a slow flow of D₂O was passed into the tube while the spectrum was recorded. Twenty-five scans were taken over 40 min and co-added.

3. Results

The ground state rovibrational transitions for the four most abundant isotopomers of barium hydride, ¹³⁸BaH, ¹³⁷BaH, ¹³⁶BaH and ¹³⁵BaH, with natural abundances, 71.7%, 11.2%, 7.9% and 6.6%, respectively, were recorded in emission. The rovibrational transitions for each isotopic species of BaH appear as doublets, because of the coupling of the unpaired electron spin to the total rotational angular momentum. The doublet pattern and the set of peaks for each isotopic species of BaH are shown in the R(11) fundamental transition (figure 1).

The line positions were measured using PC-Decomp, a program developed by J. Brault of the National Solar Observatory at Kitt Peak. The peaks were fitted to Voigt lineshape functions to determine the line positions. These are reported for each isotopic species with observed minus calculated values from the fit to Dunham parameters, in parentheses, in tables 1–4.

The calibration spectrum of D₂O was observed at the same temperature as BaH, but in absorption. The line positions were measured using PC-Decomp, and the resulting values were compared with the wavenumber standards produced by Camy-Peyret *et al.* [6]. No systematic deviation was found in the measured line positions and the residuals were found to be within reasonable limits, so no calibration of the data was needed.

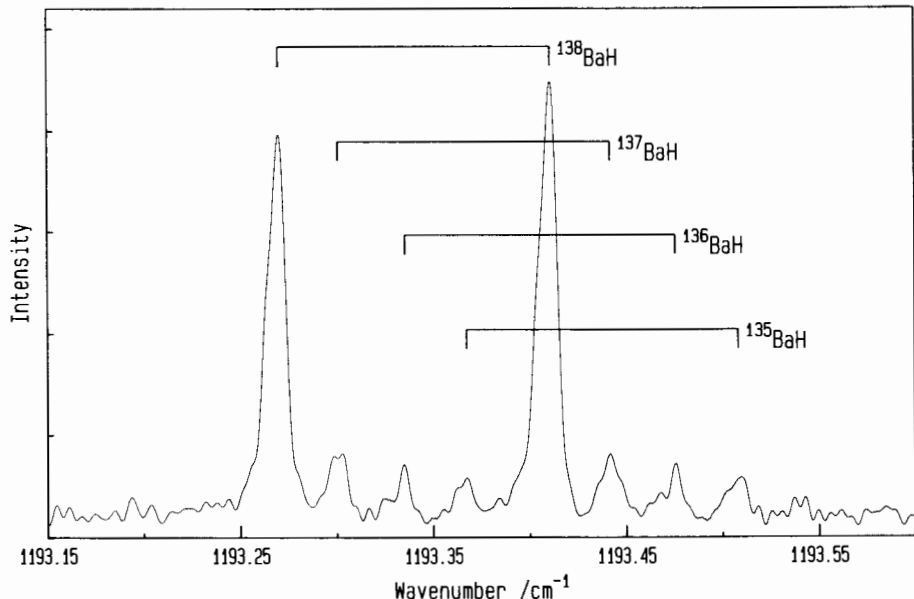


Figure 1. A portion of the vibration-rotation emission spectrum of BaH. The R(11) transition of the fundamental band is shown.

The line positions for each isotopomer were each fitted to the usual energy level expression [7]

$$F_v(J) = T_v + B_v N(N+1) - D_v[N(N+1)]^2 + H_v[N(N+1)]^3,$$

with terms to include spin-rotation coupling

$$+ \frac{N}{2}(\gamma + \gamma_D N(N+1)) \quad \text{for } J = N + \frac{1}{2}$$

$$- \frac{N+1}{2}(\gamma + \gamma_D N(N+1)) \quad \text{for } J = N - \frac{1}{2}$$

where T_v is the vibrational term energy, B_v , D_v , and H_v are the rotational constants, N is the rotational quantum number, and γ and γ_D are the spin-rotation constants. The parameters determined for ^{138}BaH are reported in table 5. For the three minor isotopes, γ_D was fixed to the value calculated using the isotope relation:

$$\gamma_D^* = \left(\frac{\mu}{\mu^*} \right)^2 \gamma_D$$

where μ and γ_D are the reduced mass and spin-rotation constant for the ^{138}BaH isotope and μ^* and γ_D^* are the reduced mass and spin-rotation constant for the isotope. The molecular constants determined for ^{137}BaH , ^{136}BaH , and ^{135}BaH are reported in table 6.

The line positions for each isotopomer were also fitted to the Dunham energy level expression [8]

$$F_{vN} = \sum_{i,j} Y_{ij}(v + \frac{1}{2})^i [N(N+1)]^j,$$

Table 1. Observed transitions (cm^{-1}) for ^{138}BaH ; observed minus calculated are given in parentheses.

J'	v'	J''	v''	Observed/ cm^{-1}	J'	v'	J''	v''	Observed/ cm^{-1}	J'	v'	J''	v''	Observed/ cm^{-1}
22.5	1	23.5	0	957.2298(04)	5.5	1	4.5	0	1170.8390(−04)	19.5	2	20.5	1	957.3763(08)
21.5	1	22.5	0	957.5111(−17)	6.5	1	5.5	0	1182.2718(02)	18.5	2	19.5	1	957.6480(41)
21.5	1	22.5	0	966.1433(−54)	7.5	1	6.5	0	1182.4239(−05)	18.5	2	19.5	1	965.9415(13)
20.5	1	21.5	0	966.4289(−08)	7.5	1	6.5	0	1187.8451(−05)	17.5	2	18.5	1	966.2052(−00)
20.5	1	21.5	0	974.9946(−13)	8.5	1	7.5	0	1187.9922(−07)	17.5	2	18.5	1	974.4220(−12)
19.5	1	20.5	0	983.7651(−04)	8.5	1	7.5	0	1193.2676(06)	16.5	2	17.5	1	974.6845(−02)
18.5	1	19.5	0	984.0380(−09)	9.5	1	8.5	0	1193.4079(−07)	16.5	2	17.5	1	982.8231(10)
18.5	1	19.5	0	992.4556(02)	9.5	1	8.5	0	1198.5338(08)	15.5	2	16.5	1	983.0804(04)
17.5	1	18.5	0	992.7259(−04)	10.5	1	9.5	0	1198.6685(−03)	15.5	2	16.5	1	991.1345(01)
17.5	1	18.5	0	1001.0638(−00)	10.5	1	9.5	0	1203.6395(−17)	14.5	2	15.5	1	991.3880(−06)
16.5	1	17.5	0	1001.3320(−02)	11.5	1	10.5	0	1203.7710(−03)	14.5	2	15.5	1	999.3575(−01)
16.5	1	17.5	0	1009.5815(−01)	11.5	1	10.5	0	1208.5897(07)	13.5	2	14.5	1	999.6086(07)
15.5	1	16.5	0	1009.8558(04)	12.5	1	11.5	0	1208.7132(−01)	13.5	2	14.5	1	1007.4886(−04)
15.5	1	16.5	0	1018.0310(−00)	12.5	1	11.5	0	1213.3748(07)	12.5	2	13.5	1	1007.7358(02)
14.5	1	15.5	0	1018.2904(03)	13.5	1	12.5	0	1213.4915(−10)	12.5	2	13.5	1	1015.5258(−04)
14.5	1	15.5	0	1026.3819(02)	13.5	1	12.5	0	1217.9956(16)	11.5	2	12.5	1	1015.7687(−01)
13.5	1	14.5	0	1026.6372(02)	14.5	1	13.5	0	1218.1057(−06)	11.5	2	12.5	1	1023.4656(−09)
13.5	1	14.5	0	1034.6412(03)	14.5	1	13.5	0	1222.4468(05)	10.5	2	11.5	1	1023.7044(−06)
12.5	1	13.5	0	1034.8927(03)	15.5	1	14.5	0	1222.5515(−10)	10.5	2	11.5	1	1031.3065(−07)
12.5	1	13.5	0	1042.8068(06)	15.5	1	14.5	0	1226.7288(03)	9.5	2	10.5	1	1031.5421(03)
11.5	1	12.5	0	1043.0549(11)	16.5	1	15.5	0	1226.8278(−08)	9.5	2	10.5	1	1039.0456(−02)
11.5	1	12.5	0	1050.8751(02)	16.5	1	15.5	0	1230.8393(08)	8.5	2	9.5	1	1039.2759(−04)
10.5	1	11.5	0	1051.1191(06)	17.5	1	16.5	0	1230.9324(02)	8.5	2	9.5	1	1046.6794(−03)
10.5	1	11.5	0	1058.8446(01)	17.5	1	16.5	0	1234.7743(04)	7.5	2	8.5	1	1046.9054(−05)
9.5	1	10.5	0	1059.0844(04)	18.5	1	17.5	0	1234.8620(08)	7.5	2	8.5	1	1054.2055(−06)
9.5	1	10.5	0	1066.7121(−01)	18.5	1	17.5	0	1238.5327(03)	6.5	2	7.5	1	1054.4271(−09)
8.5	1	9.5	0	1066.9477(02)	19.5	1	18.5	0	1238.6130(−04)	6.5	2	7.5	1	1061.6220(−03)
8.5	1	9.5	0	1074.4734(01)	19.5	1	18.5	0	1242.1111(−08)	5.5	2	6.5	1	1061.8392(−06)
7.5	1	8.5	0	1074.7065(00)	20.5	1	19.5	0	1242.1854(−09)	5.5	2	6.5	1	1068.9250(−07)
7.5	1	8.5	0	1082.1302(−11)	20.5	1	19.5	0	1245.5100(−02)	4.5	2	5.5	1	1069.1399(12)
6.5	1	7.5	0	1082.3586(05)	21.5	1	20.5	0	1245.5765(−16)	4.5	2	5.5	1	1076.1134(−01)
6.5	1	7.5	0	1089.6773(−01)	21.5	1	20.5	0	1248.7256(03)	3.5	2	4.5	1	1076.3222(02)

Table 1. (continued)

J'	v'	J''	v''	Observed/cm ⁻¹	J'	v'	J''	v''	Observed/cm ⁻¹	J'	v'	J''	v''	Observed/cm ⁻¹
5.5	1	6.5	0	1089·9000(02)	22.5	1	21.5	0	1248·7869(04)	3.5	2	4.5	1	1083·1841(09)
5.5	1	6.5	0	1097·1102(-08)	22.5	1	21.5	0	1251·7558(07)	2.5	2	3.5	1	1083·3868(-03)
5.5	1	5.5	0	1097·3288(-02)	23.5	1	22.5	0	1251·8093(-03)	2.5	2	3.5	1	1090·1319(00)
4.5	1	5.5	0	1104·4287(-06)	23.5	1	22.5	0	1254·5974(-02)	1.5	2	2.5	1	1090·3320(10)
4.5	1	5.5	0	1104·6420(-07)	24.5	1	23.5	0	1254·6446(-07)	1.5	2	2.5	1	1096·9535(-35)
3.5	1	4.5	0	1110·2500(03)	24.5	1	23.5	0	1257·2500(-09)	2.5	2	1.5	1	1123·1421(12)
3.5	1	4.5	0	1111·8380(-04)	25.5	1	24.5	0	1257·2903(-15)	2.5	2	1.5	1	1129·1344(15)
2.5	1	3.5	0	1118·7085(-07)	25.5	1	24.5	0	1259·7135(03)	3.5	2	2.5	1	1129·3025(04)
2.5	1	3.5	0	1118·9139(06)	26.5	1	25.5	0	1259·7473(02)	3.5	2	2.5	1	1135·1591(-02)
1.5	1	2.5	0	1125·6673(20)	26.5	1	25.5	0	1261·9815(-11)	4.5	2	3.5	1	1135·3229(05)
1.5	1	2.5	0	1152·3768(-43)	27.5	1	26.5	0	1262·0095(00)	4.5	2	3.5	1	1141·0444(10)
2.5	1	1.5	0	1158·6740(-04)	27.5	1	26.5	0	1264·0564(-10)	5.5	2	4.5	1	1141·2018(-04)
3.5	1	2.5	0	1164·6590(-01)	28.5	1	27.5	0	1264·0761(-10)	7.5	2	6.5	1	1152·5219(04)
3.5	1	2.5	0	1164·8285(04)	28.5	1	27.5	0	1265·9361(01)	7.5	2	6.5	1	1157·8148(02)
4.5	1	3.5	0	1164·8285(04)	29.5	1	28.5	0	1265·9465(-19)	8.5	2	7.5	1	1157·9569(-00)
4.5	1	3.5	0	1170·6761(04)	—	—	—	—	—	—	—	—	—	—
—	—	—	—	—	—	—	—	—	—	—	—	—	—	1142·9441(-03)
8.5	2	7.5	1	1163·1031(03)	12.5	3	13.5	2	988·4150(-15)	10.5	3	9.5	2	—
9.5	2	8.5	1	1163·2396(02)	11.5	3	12.5	2	988·6530(-11)	11.5	3	10.5	2	1143·0652(07)
9.5	2	8.5	1	1168·2351(-04)	11.5	3	12.5	2	996·2266(-14)	11.5	3	10.5	2	1147·6225(03)
10.5	2	9.5	1	1168·3657(-06)	10.5	3	11.5	2	996·4614(-03)	12.5	3	11.5	2	1147·7385(-06)
10.5	2	9.5	1	1173·2100(-02)	10.5	3	11.5	2	1003·9404(06)	12.5	3	11.5	2	1152·1427(04)
11.5	2	10.5	1	1173·3357(04)	9.5	3	10.5	2	1004·1704(09)	13.5	3	12.5	2	1152·2518(13)
11.5	2	10.5	1	1178·0244(-01)	9.5	3	10.5	2	1011·5485(-08)	13.5	3	12.5	2	1156·4920(-22)
12.5	2	11.5	1	1178·1436(-01)	8.5	3	9.5	2	1011·7731(-16)	14.5	3	13.5	2	1156·5964(-02)
12.5	2	11.5	1	1182·6754(-04)	8.5	3	9.5	2	1019·0561(26)	14.5	3	13.5	2	1160·6775(-08)
13.5	2	12.5	1	1182·7902(11)	7.5	3	8.5	2	1019·2767(19)	15.5	3	14.5	2	1160·7720(-25)
13.5	2	12.5	1	1187·1624(06)	7.5	3	8.5	2	1026·4537(36)	15.5	3	14.5	2	1164·6893(-30)
14.5	2	13.5	1	1187·2685(-06)	6.5	3	7.5	2	1026·6661(-09)	16.5	3	15.5	2	1164·7822(-01)
14.5	2	13.5	1	1191·4800(-01)	6.5	3	7.5	2	1033·7376(14)	16.5	3	15.5	2	1168·5318(-20)
14.5	2	14.5	1	1191·5807(-06)	5.5	3	6.5	2	1033·9519(32)	17.5	3	16.5	2	1168·6174(-02)
15.5	2	14.5	1	1195·6277(-07)	5.5	3	6.5	2	1040·9088(-05)	17.5	3	16.5	2	1172·1957(-48)
15.5	2	14.5	1	1195·7242(09)	4.5	3	5.5	2	1041·1156(-17)	18.5	3	17.5	2	1172·2787(08)

Table 1. (continued)

J'	v'	J''	v''	Observed/cm $^{-1}$	J'	v'	J''	v''	Observed/cm $^{-1}$	J'	v'	J''	v''	Observed/cm $^{-1}$
16.5	2	15.5	1	1199.6038(-03)	4.5	3	5.5	2	1047.9684(20)	19.5	3	18.5	2	1179.0001(-07)
17.5	2	16.5	1	1199.6931(02)	3.5	3	4.5	2	1048.1711(11)	20.5	3	19.5	2	1179.0652(-01)
17.5	2	16.5	1	1203.4055(03)	2.5	3	3.5	2	1055.1088(47)	20.5	3	19.5	2	1182.1300(-00)
18.5	2	17.5	1	1203.4886(09)	2.5	3	3.5	2	1061.7240(12)	21.5	3	20.5	2	1182.1869(-11)
18.5	2	17.5	1	1207.0300(05)	1.5	3	2.5	2	1061.9199(29)	21.5	3	20.5	2	1185.0726(-34)
19.5	2	18.5	1	1207.1069(14)	2.5	3	1.5	2	1099.9399(75)	22.5	3	21.5	2	1185.1293(20)
19.5	2	18.5	1	1210.4771(24)	3.5	3	2.5	2	1100.0999(31)	23.5	3	22.5	2	1190.4031(-67)
20.5	2	19.5	1	1210.5459(18)	3.5	3	2.5	2	1105.8308(45)	24.5	3	23.5	2	1190.4412(-64)
21.5	2	20.5	1	1213.8049(34)	4.5	3	3.5	2	1105.9883(28)	24.5	3	23.5	2	1192.7934(-03)
21.5	2	20.5	1	1216.8246(54)	4.5	3	3.5	2	1111.5797(20)	25.5	3	24.5	2	1192.8264(17)
22.5	2	21.5	1	1216.8771(16)	5.5	3	4.5	2	1111.7343(29)	25.5	3	24.5	2	1194.9835(-31)
22.5	2	21.5	1	1219.7188(43)	5.5	3	4.5	2	1117.1864(27)	26.5	3	25.5	2	1195.0173(68)
23.5	2	22.5	1	1219.7682(42)	6.5	3	5.5	2	1117.3360(40)	26.5	3	25.5	2	1196.9828(-38)
24.5	2	23.5	1	1224.9464(52)	6.5	3	5.5	2	1122.6426(07)	27.5	3	26.5	2	1197.0025(-10)
25.5	2	24.5	1	1224.9837(67)	7.5	3	6.5	2	1122.7873(26)	27.5	3	26.5	2	1198.7999(80)
25.5	2	24.5	1	1227.2786(97)	7.5	3	6.5	2	1127.9495(-00)	28.5	3	27.5	2	1198.8026(09)
26.5	2	25.5	1	1227.3051(74)	8.5	3	7.5	2	1128.0880(11)	28.5	3	27.5	2	1200.3949(-61)
14.5	3	15.5	2	972.5028(-14)	8.5	3	7.5	2	1133.1039(-03)	29.5	3	28.5	2	1200.4104(69)
13.5	3	14.5	2	972.7461(-35)	9.5	3	8.5	2	1133.2355(-04)	29.5	3	28.5	2	1201.8125(03)
13.5	3	14.5	2	980.5072(-05)	9.5	3	8.5	2	1138.1029(-04)	30.5	3	29.5	2	1203.0239(-01)
12.5	3	13.5	2	980.7479(-13)	10.5	3	9.5	2	1138.2302(09)					

Table 2. Observed transitions (cm^{-1}) for ^{137}BaH ; observed minus calculated are given in parentheses.

J'	v'	J''	v''	Observed/ cm^{-1}	J'	v'	J''	v''	Observed/ cm^{-1}	J'	v'	J''	v''	Observed/ cm^{-1}
16.5	1	17.5	0	1009.6174(13)	4.5	1	5.5	0	1104.4571(04)	11.5	1	10.5	0	1208.6242(22)
14.5	1	15.5	0	1026.4076(06)	3.5	1	4.5	0	1104.6715(-01)	12.5	1	11.5	0	1208.7450(-16)
13.5	1	14.5	0	1034.6652(-14)	3.5	1	4.5	0	1111.6595(23)	12.5	1	11.5	0	1213.4077(04)
12.5	1	13.5	0	1034.9171(-10)	2.5	1	3.5	0	1111.8748(73)	13.5	1	12.5	0	1213.5180(-77)
12.5	1	13.5	0	1042.8324(03)	2.5	1	3.5	0	1118.7363(-08)	13.5	1	12.5	0	1218.0264(-11)
11.5	1	12.5	0	1043.0794(-05)	1.5	1	2.5	0	1118.9426(-02)	14.5	1	13.5	0	1218.1350(-46)
11.5	1	12.5	0	1050.9010(-00)	3.5	1	2.5	0	1158.7083(24)	15.5	1	14.5	0	1222.5853(-06)
10.5	1	11.5	0	1051.1453(03)	4.5	1	3.5	0	1164.8586(-13)	15.5	1	14.5	0	1226.7643(17)
10.5	1	11.5	0	1058.8713(06)	4.5	1	3.5	0	1170.7052(-11)	16.5	1	15.5	0	1226.8610(-09)
9.5	1	10.5	0	1059.1109(01)	5.5	1	4.5	0	1170.8738(24)	16.5	1	15.5	0	1230.8728(-01)
9.5	1	10.5	0	1066.7381(-04)	5.5	1	4.5	0	1176.5783(-01)	17.5	1	16.5	0	1230.9666(10)
8.5	1	9.5	0	1066.9705(-43)	6.5	1	5.5	0	1176.7396(16)	18.5	1	17.5	0	1234.8949(03)
8.5	1	9.5	0	1074.4999(-20)	6.5	1	5.5	0	1182.3022(-08)	20.5	1	19.5	0	1242.2203(03)
7.5	1	8.5	0	1074.7356(16)	7.5	1	6.5	0	1182.4567(-03)	20.5	1	19.5	0	1245.5471(07)
7.5	1	8.5	0	1082.1584(03)	8.5	1	7.5	0	1193.2977(-13)	21.5	1	20.5	0	1245.6119(-01)
6.5	1	7.5	0	1082.3818(-42)	9.5	1	8.5	0	1193.4415(01)	21.5	1	20.5	0	1248.7687(65)
6.5	1	7.5	0	1089.7045(02)	9.5	1	8.5	0	1198.5664(11)	22.5	1	21.5	0	1248.8247(40)
5.5	1	6.5	0	1089.9258(-23)	10.5	1	9.5	0	1198.7003(-16)	22.5	1	21.5	0	1251.7876(-52)
5.5	1	6.5	0	1097.1389(08)	10.5	1	9.5	0	1203.6752(14)	23.5	1	22.5	0	1251.8429(-12)
4.5	1	5.5	0	1097.3564(-11)	11.5	1	10.5	0	1203.8058(14)					

Table 3. Observed transitions (cm^{-1}) for ^{136}BaH ; observed minus calculated are given in parentheses.

J'	v'	J''	v''	Observed/ cm^{-1}	J'	v'	J''	v''	Observed/ cm^{-1}	J'	v'	J''	v''	Observed/ cm^{-1}
16.5	1	17.5	0	1009.6368(08)	5.5	1	6.5	0	1089.9535(-05)	10.5	1	9.5	0	1198.7344(19)
15.5	1	16.5	0	1009.9017(10)	4.5	1	5.5	0	1097.3816(-21)	10.5	1	9.5	0	1203.7075(15)
15.5	1	16.5	0	1018.0715(-52)	4.5	1	5.5	0	1104.4857(07)	11.5	1	10.5	0	1203.8329(-25)
14.5	1	15.5	0	1018.3374(-00)	2.5	1	3.5	0	1111.8965(22)	11.5	1	10.5	0	1208.6542(-01)
14.5	1	15.5	0	1026.4280(-06)	2.5	1	3.5	0	1118.7663(01)	12.5	1	11.5	0	1208.7788(09)
13.5	1	14.5	0	1034.6894(04)	1.5	1	2.5	0	1118.9674(-24)	12.5	1	11.5	0	1213.4437(40)
12.5	1	13.5	0	1034.9430(14)	2.5	1	1.5	0	1158.5633(23)	13.5	1	12.5	0	1213.5586(12)
12.5	1	13.5	0	1042.8557(04)	3.5	1	2.5	0	1158.7375(32)	13.5	1	12.5	0	1218.0633(35)
11.5	1	12.5	0	1043.1009(-29)	3.5	1	2.5	0	1164.7191(-14)	14.5	1	13.5	0	1218.1744(27)
11.5	1	12.5	0	1050.9265(15)	4.5	1	3.5	0	1164.8844(-42)	14.5	1	13.5	0	1222.5135(11)
10.5	1	11.5	0	1051.1691(-02)	4.5	1	3.5	0	1170.7416(40)	15.5	1	14.5	0	1222.6180(-03)
10.5	1	11.5	0	1058.8979(25)	5.5	1	4.5	0	1170.9008(04)	15.5	1	14.5	0	1226.7941(-08)
9.5	1	10.5	0	1059.1389(35)	5.5	1	4.5	0	1176.6127(28)	16.5	1	15.5	0	1226.8973(26)
9.5	1	10.5	0	1066.7653(13)	6.5	1	5.5	0	1176.7672(-01)	16.5	1	15.5	0	1230.9038(-12)
8.5	1	9.5	0	1066.9963(-34)	6.5	1	5.5	0	1182.3347(01)	17.5	1	16.5	0	1230.9959(-28)
8.5	1	9.5	0	1074.5246(-34)	7.5	1	6.5	0	1182.4873(08)	18.5	1	17.5	0	1234.9266(-15)
7.5	1	8.5	0	1074.7597(04)	8.5	1	7.5	0	1188.0546(-09)	20.5	1	19.5	0	1242.2499(-40)
7.5	1	8.5	0	1082.1810(-39)	8.5	1	7.5	0	1193.3330(21)	22.5	1	21.5	0	1248.8567(22)
6.5	1	7.5	0	1082.4021(-95)	9.5	1	8.5	0	1193.4695(-22)	23.5	1	22.5	0	1251.8775(-03)
6.5	1	7.5	0	1089.7269(-48)	9.5	1	8.5	0	1198.5967(-06)					

Table 4. Observed transitions (cm^{-1}) for ^{135}BaH ; observed minus calculated are given in parentheses.

Table 5. Molecular constants for observed transitions of ^{138}BaH isotopomer (cm^{-1}).

Constant	$v = 0$	$v = 1$	$v = 2$	$v = 3$
T_v	—	1139.28973(11)	2249.60638(15)	3331.11942(21)
B_v	3.3496069(48) ^a	3.2838210(42)	3.2179128(41)	3.1518809(44)
$10^3 D_v$	0.112778(19)	0.112474(16)	0.112112(15)	0.111749(14)
$10^9 H_v$	3.070(22)	3.072(17)	3.049(15)	3.026(13)
γ	0.192092(89)	0.18707(87)	0.182098(88)	0.177145(88)
$10^6 \gamma_D$	-13.17(15)	-13.10(13)	-13.11(13)	-12.90(12)

^aOne standard deviation in parentheses.

Table 6. Molecular constants for observed minor isotopes of BaH (cm^{-1}).

Constant	^{137}BaH	^{136}BaH	^{135}BaH
B_0	3.349 845(53) ^a	3.349 991(69)	3.350 245(83)
$10^3 D_0$	0.113 29(34)	0.113 07(43)	0.113 23(50)
$10^9 H_0$	3.78(67)	3.47(81)	3.39(83)
γ_0	0.191 99(52)	0.191 5(63)	0.193 28(92)
$10^6 \gamma_{D0}$	-13.1 ^b	-13.1 ^b	-13.1 ^b
T_1	1139.321 08(68)	1139.348 15(83)	1139.377 8(15)
B_1	3.284 015(48)	3.284 207(64)	3.284 482(80)
$10^3 D_1$	0.112 76(29)	0.112 82(36)	0.113 18(47)
$10^9 H_1$	3.45(52)	3.52(62)	3.81(72)
γ_1	0.186 98(50)	0.186 42(63)	0.188 36(95)
$10^6 \gamma_{D1}$	-13.1 ^b	-13.1 ^b	-13.1 ^b

^aOne standard deviation in parentheses.^bFixed to values calculated using isotope relationships (see text).

with terms added for spin-rotation coupling [5]

$$+\frac{N}{2} \sum_{ij} \gamma_{ij}(v + \frac{1}{2})^j [N(N+1)]^{j-1} \quad \text{for } J = N + \frac{1}{2}$$

$$-\frac{(N+1)}{2} \sum_{ij} \gamma_{ij} (v + \frac{1}{2})^j [N(N+1)]^{j-1} \quad \text{for } J = N - \frac{1}{2}$$

where v and N are the vibration and rotation quantum numbers, respectively, and γ_{ij} are the Dunham coefficients which are related to the molecular constants for the isotopic species. Since only the fundamental transitions were observed for the three minor isotopic species, data obtained by Magg *et al.* [5] for the two hot band transitions were used in the fit. The Dunham parameters determined for the four isotopomers are reported in table 7. The complete spectral coverage of the Fourier transform spectrometer and the improved precision of the line positions result in Dunham constants for ^{138}BaH that are more accurate by a factor of ten than those reported by Magg *et al.*

Table 7. Dunham constants for observed BaH isotopomers (cm^{-1}).

Coefficient	^{138}BaH	^{137}BaH	^{136}BaH	^{135}BaH
Y_{10}	1168.424 51(23) ^a	1168.443 7(11)	1168.474 7(17)	1168.504 6(27)
Y_{20}	-14.612 59(13)	-14.605 71(57)	-14.606 91(80)	-14.605 7(13)
Y_{30}	0.027 928(23)	0.026 946(93)	0.027 04(13)	0.026 67(22)
Y_{01}	3.382 449 9(34)	3.382 612(25)	3.382 754(29)	3.383 030(69)
Y_{11}	-0.065 686 27(61)	-0.065 678 5(60)	-0.065 690(11)	-0.065 704(19)
$10^3 Y_{21}$	-0.052 87(10)	-0.055 78(95)	-0.053 1(20)	-0.052 9(42)
$10^3 Y_{02}$	-0.112 889 1(93)	-0.113 011(98)	-0.112 88(15)	-0.113 23(42)
$10^6 Y_{12}$	0.318 7(14)	0.303(23)	0.301(29)	0.313(36)
$10^9 Y_{03}$	3.001(10)	3.23(18)	3.08(28)	3.37(69)
γ_{01}	0.194 512(94)	0.196 19(42)	0.193 73(48)	0.195 36(78)
$10^3 \gamma_{11}$	-4.974 6(46)	-4.977(35)	-5.027(36)	-4.959(49)
$10^3 \gamma_{02}$	-0.012 99(12)	-0.016 0(11)	-0.011 0(13)	-0.013 2(18)

^aOne standard deviation in parentheses.

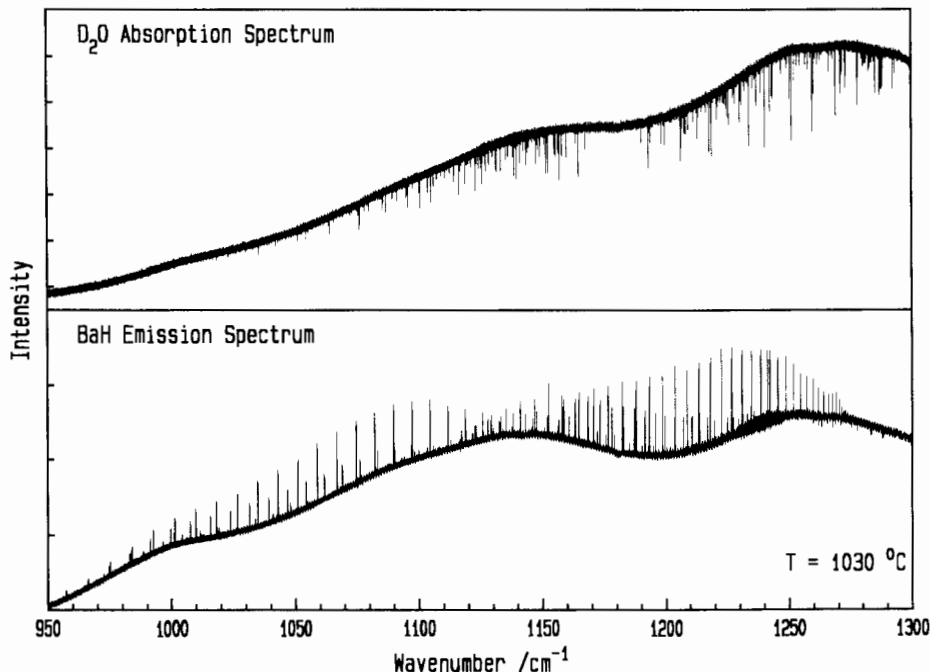
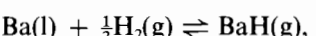


Figure 2. A comparison of the D_2O absorption spectrum and the BaH emission spectrum recorded under similar experimental conditions.

The concentration of BaH in the gas phase in the tube furnace was estimated by thermodynamic calculations. The equation for the formation of barium monohydride is shown below:



where the elements are written in their standard states at 1300 K. The free energy of formation ΔG_f^0 of this reaction is

$$\begin{aligned} \Delta G_f^0 &= \Delta H_f^0 - T\Delta S_f^0 \\ &= 158 \text{ kJ/mole} - 1300 \text{ K}(5.37 \times 10^{-2} \text{ kJ/(mole K)}) \\ &= 88.1 \text{ kJ mol}^{-1} \end{aligned}$$

The equilibrium constant $K = 2.87 \times 10^{-4}$, was calculated from the equation

$$\Delta G_f^0 = -RT \ln K.$$

The thermodynamic data for these calculations were taken from the JANAF Thermochemical Tables [9], and the dissociation energy $D = 1.95 \text{ eV}$, for BaH , from Huber and Herzberg [10]. Since the pressure of H_2 in the tube was known to be 20 Torr, the partial pressure of BaH was estimated to be 35 mTorr.

A sample at 35 mTorr in a path length of less than 80 cm gave a spectrum with signal-to-noise ratio of 25 for the strongest lines. The sensitivity of infrared emission is demonstrated by comparing the D_2O absorption spectrum and the BaH emission spectrum (figure 2). The D_2O spectrum was recorded while there were still Ba metal and hydrogen present at 1030 °C in the furnace. The lack of BaH absorption lines in the D_2O spectrum demonstrates that a lower concentration of BaH is required to

produce an emission spectrum than to produce an absorption spectrum for our experimental conditions. Infrared emission spectroscopy is, therefore, at least a factor of 10 more sensitive than traditional absorption spectroscopy in this case.

4. Conclusion

The rovibrational infrared emission spectra of the four most abundant isotopic species of BaH were recorded with a Fourier transform spectrometer. Infrared spectra of BaH had been observed in the past in absorption using a diode laser spectrometer. The Fourier transform measurements have wider spectral coverage and greater accuracy than the diode laser work. Fourier transform emission spectroscopy is a promising technique for observing rovibrational spectra of high temperature free radical molecules at long wavelengths.

This work was supported by the Natural Sciences and Engineering Research Council of Canada and the Phillips Laboratory/Propulsion Directorate, Edwards Air Force Base. Acknowledgement is made to the Petroleum Research Fund, administered by the American Chemical Society, for partial support of this work. Support was also provided by URIF. One of us (H.G.H.) thanks the Deutsche Forschungsgemeinschaft for a postdoctoral scholarship.

References

- [1] FREDRICKSON, W. R., and WATSON, W. W., 1932, *Phys. Rev.*, **39**, 753.
- [2] APPELBLAD, O., BERG, L. -E., KLYNNING, L., and JOHNS, J. W. C., 1985, *Phys. Scripta*, **31**, 69.
- [3] BERNARD, A., EFFANTIN, C., d'INCAN, J., FABRE, G., STRINGAT, R., and BARROW, R. F., 1989, *Molec. Phys.*, **67**, 1.
- [4] ALLOUCHE, A. R., NICHOLAS, G., BARTHELAT, J. C., and SPIEGELMANN, F., 1992, *J. Chem. Phys.*, **96**, 7646.
- [5] MAGG, U., BIRK, H., and JONES, H., 1988, *Chem. Phys. Lett.*, **149**, 321.
- [6] CAMY-PETRET, C., FLAUD, J. -M., MAHMOUDI, A., GUELACHVILI, G., and JOHNS, J. W. C., 1985, *Int. J. Infrared Millimeter Waves*, **6**, 199.
- [7] TOWNES, C. H., and SCHAWLOW, A. L., 1975, *Microwave Spectroscopy* (Dover).
- [8] DUNHAM, J. L., 1932, *Phys. Rev.*, **41**, 721.
- [9] CHASE, M. W. *et al.*, 1986, *JANAF Thermochemical Tables*, (ACS and AIP for the National Bureau of Standards, Washington, DC).
- [10] HUBER, K. P., and HERZBERG, G., 1979, *Constants of Diatomic Molecules* (Van Nostrand Reinhold).